*Int. J. Heat Mass Transfer.* Vol. 37, No. 2, pp. 269–282, 1994
Printed in Great Britain

0017–9310/94 $6.00 + 0.00


# Effects of interaction between adjacent free surface planar jets on local heat transfer from the impingement surface

S. J. SLAYZAK, R. VISKANTA and F. P. INCROPERA
Heat Transfer Laboratory, School of Mechanical Engineering, Purdue University, West Lafayette, IN 47907, U.S.A.

(*Received* 3 *March* 1993 *and in final form* 14 *June* 1993)

**Abstract**—Experiments have been conducted to obtain single-phase, local convection heat transfer coefficient distributions along a constant heat flux surface experiencing impingement by two, planar, free-surface jets of water. Nozzle widths and nozzle-to-heater separation distances were fixed at 5.1 and 89.7 mm, respectively, while two nozzle-to-nozzle pitches (81 and 51 mm) were considered. The ratio of impingement velocities for the two nozzles, $V^*$, was varied from 0.47 to 1.0. Interacting wall jets created by the impinging jets yielded a strong upwelling of spent flow (an *interaction fountain*), beneath which convection coefficients were comparable to those associated with the jet impingement regions. With decreasing $V^*$, impingement heat transfer coefficients beneath the weaker jet were reduced by the effects of crossflow imposed by the stronger jet.

## INTRODUCTION

JET IMPINGEMENT heat transfer has long been an area of active research, and with an ever increasing scope of applications, the field continues to attract a good deal of attention. Historically, research has primarily been concerned with gaseous (submerged) jets, operating independently or in array, and a review of the extensive literature published prior to 1979 has been provided by Martin [1]. Results of particular interest to this study relate to arrays of jets and the effect of flow interactions on local heat transfer. Secondary maxima in transport coefficients have been reported to characterize the interaction zones, and in some cases to be comparable to primary maxima associated with the impingement regions [2–4]. Similar results were obtained in more recent studies [5–8], which also showed the secondary peaks to increase with increasing Reynolds number and decreasing nozzle-to-nozzle spacing, thereby suggesting that enhancement is related to the amount of momentum retained by the interacting wall jets.

More recently, interest in high heat flux applications related to electronic cooling and materials processing has shifted the focus of attention to submerged and free-surface liquid jets. However, although much is being done to study hydrodynamic and thermal conditions associated with a single jet, comparatively little has been done to study the effects of interactions in an array of liquid jets. In fact, only one such study could be identified [9]. Local heat transfer variations produced by two, interacting free-surface circular jets were considered, with emphasis placed on conditions at the *secondary stagnation point* associated with the interaction between opposing wall jets. The authors report that the interaction zone does not appreciably affect local heat transfer associated with a single wall jet, if the interacting flows have already undergone transition to turbulence. However, substantial heat transfer enhancement did occur when the interaction preceded transition within the wall jets.

This study was motivated by the growing importance of free-surface liquid jets in high temperature materials processing, such as the cooling of hot rolled steel, and, in particular, by the application of arrays of such jets. The study focuses on the interaction between two planar, free-surface jets and on local convection coefficients in the interaction zone. For an impingement surface at which a uniform heat flux was maintained, experiments were performed for slot nozzles of fixed width (5.1 mm) and heat above the surface (89.7 mm). Jet impingement velocities were varied over the range $2.1 \leqslant \bar{V}_j \leqslant 4.5$ m s$^{-1}$, as was the ratio of velocities associated with the two nozzles ($0.47 \leqslant V^* \leqslant 1.0$). Two nozzle pitches (51 and 81 mm) were also considered.

## EXPERIMENTAL PROCEDURES

The heater module of this study was identical to that used by Vader *et al.* [10] and consisted of a 0.66 mm thick Ni–Cr–W–Mo impingement plate, which was ohmically heated to achieve a uniform heat flux. To maintain the highest plate temperature without inducing boiling, the heat flux was fixed at 0.5 MW m$^{-2}$ for all of the experiments. The plate was 260 mm long by 35.7 mm wide, and temperature measurements were made on its bottom surface by an array of 21 thermocouples. The thermocouples were spring-loaded against the surface, and a silicone

## NOMENCLATURE

| | |
|---|---|
| $A_n$ | cross sectional area of nozzle |
| $D_h$ | hydraulic diameter, $4A_n/S$ |
| $h$ | local convection heat transfer coefficient |
| $h_0$ | stagnation line heat transfer coefficient |
| $\bar{h}$ | average convection heat transfer coefficient |
| $k$ | thermal conductivity of the fluid |
| $L$ | distance along the heater surface |
| $P$ | $x$-displacement between nozzle exits (nozzle pitch) |
| $Pr$ | Prandtl number of fluid |
| $q''$ | local surface heat flux |
| $Re_D$ | Reynolds number, $\bar{V}_n D_h/\nu$ |
| $Re_j$ | Reynolds number of the jet, $\bar{V}_j w_j/\nu$ |
| $S$ | wetted perimeter of a nozzle |
| $T_f$ | fluid temperature |
| $T_w$ | temperature of the heated impingement surface |
| $\bar{V}_n$ | average jet velocity at the nozzle discharge |
| $\bar{V}_j$ | average jet impingement velocity |
| $\bar{V}_{jl}$ | average impingement velocity for jet on the left |
| $\bar{V}_{jr}$ | average impingement velocity for jet on the right |
| $V^*$ | ratio of impingement velocities, $\bar{V}_{jr}/\bar{V}_{jl}$ |
| $w_j$ | width of the jet at impingement |
| $x$ | displacement from left nozzle midline along the impingement surface |
| $x_c$ | equilibrium position of the interaction zone. |

Greek symbols

| | |
|---|---|
| $\nu$ | kinematic viscosity. |

paste (Omegatherm 201; thermal conductivity of 2.3 W m$^{-1}$ C$^{-1}$, electrical resistivity of $10^{12}$ Ω m) was applied to each thermocouple bead to provide electrical isolation with good thermal contact. The thermocouples were positioned at 5.08 mm intervals along the midline of the plate, and for a particular operating condition, each of the 21 reported temperatures corresponded to the arithmetic mean of 100 readings taken over approximately a 12 min interval. The 100 readings of a run were taken in bursts of seven (with the first two ignored). Each burst took less than one second (i.e. the frequency within a burst was approximately 7 Hz). The time between bursts (~ 36 s) was randomly varied to reduce the effect of frequency related noise. Hence, there is no single frequency to describe the data acquisition rate.

Temperatures measured at the bottom surface of the heated impingement plate were used with a solution of the two-dimensional heat equation to obtain the temperature field within the plate and the distribution of the convection heat transfer coefficient along the impingement surface. The solution domain included 150 nodal points in the flow direction, requiring use of a cubic spline, least square procedure to interpolate associated back surface temperature from the 21 thermocouple measurements. Details of the data reduction procedure are provided by Vader *et al.* [10].

With local temperature and heat fluxes known for the impingement surface, local convection coefficients may be computed

$$h(x) = \frac{q''}{T_w(x) - T_f} \tag{1}$$

and, in turn, may be used to determine an average heat transfer coefficient for the surface

$$\bar{h} = \frac{\bar{q}''}{\Delta T} = \frac{(1/L)\int_0^L \{h(x)\cdot[T_w(x)-T_f]\}\,dx}{(1/L)\int_0^L [T_w(x)-T_f]\,dx}. \tag{2}$$

Although it is not computationally convenient for design calculations, $\bar{h}$ provides a figure of merit for determining the relative heat transfer effectiveness of single and dual jet configurations. To facilitate a comparison between single and dual jet configurations, $L$ is equated to the nozzle pitch, and $\bar{h}$ for a single jet is calculated over the same region as that for the dual jet system to which it is being compared. Note that the product of the local heat transfer coefficient and temperature difference in the numerator (the local heat flux) of equation (2) is constant for the heater. An experimental uncertainty analysis based on accepted procedures [11] yielded convection coefficient uncertainties of ±18%.

An existing plenum design [12] was modified to allow two jets to be positioned within 25 mm of each other (Fig. 1). The jet temperatures were measured just upstream of honeycomb flow straighteners and were maintained at 30 ± 0.1°C throughout the experiments. Jet flow rates were measured upstream of the plena using either of two turbine flowmeters which were accurate to within 0.5% of full scale (0.08 or 0.02 l s$^{-1}$). The flow rates were used to determine mean nozzle discharge velocities, from which impingement velocities were calculated by correcting for acceleration due to gravity while descending to the plate. The cross-section of the planar nozzles measured 5.1 mm by 127.0 mm on a side. With Reynolds numbers in the range $24\,000 \leqslant Re_D \leqslant 51\,000$ and a development

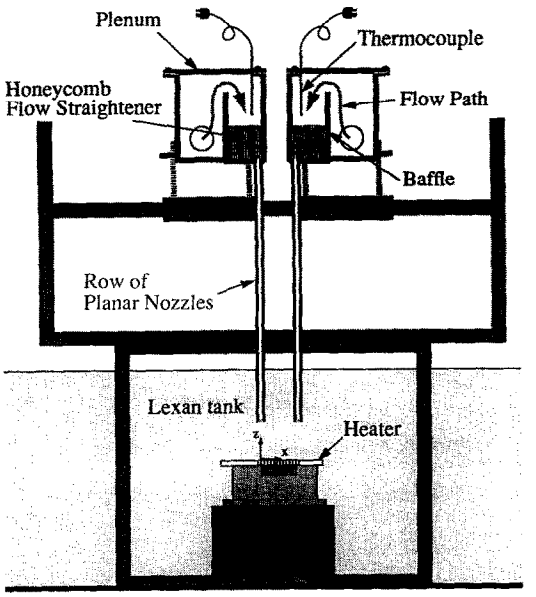


FIG. 1. Sectional view of the plena and planar nozzles positioned over the heater module.

length exceeding fifty hydraulic diameters, nozzle discharge conditions were characterized by a turbulent, fully developed velocity profile.

After impingement and bifurcation in a multi-jet system, opposing wall jets collide, forming *interaction fountains* which vigorously eject water from the plate. For the nozzle pitches considered in this study, water from the fountains impacted the free-surface jets prior to impingement. Related disturbances were of sufficient magnitude to affect momentum exchange in the wall jet interaction zone, causing the fountain to careen back and forth and to impact either jet with such force as to cause a momentary loss of coherence. To stabilize the flow field, jet guards were constructed of 3.2 mm thick acrylic and securely positioned as shown in Fig. 2. With the guards in place, the free-surface jets descended unimpeded to the plate, and oscillations of the interaction fountain were reduced to several millimeters. Moreover, the wall jets were less susceptible to disruption by spent flow reimpinging in the form of droplets.

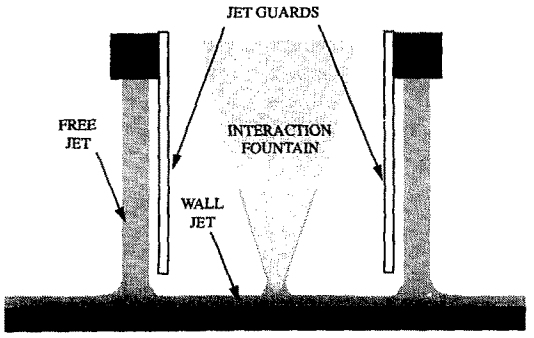


FIG. 2. Positioning of the jet guards.

To facilitate flow visualization, the heater module was replaced by an acrylic plate, which permitted visualization from below, and a flow window was installed (Fig. 3) to circumvent the deleterious effects of splashing and to facilitate visualization from the side. The flow window assembly included razor-edged splitters which allowed that part of each jet on the far side of the acrylic window to impinge normally, while diverting flow on the other side away from the line of sight. Splashing between the flow and observer was thereby avoided, and with water wetting the far side of the window, a clear view of the impingement and interaction zones was provided. The flow window was not used when viewing from below. The acrylic impingement surface was graduated in 10 mm intervals to aid in matching flow conditions with heat transfer data. The flow field was diffusely illuminated from the side and slightly above the plate and was recorded using Kodak TMAX 400 film with an aperture of f/4 at a shutter speed of 1/500 s. The impingement region was clearly defined when viewing from below, and the degree of crossflow could be determined. That is, for dissimilar jet velocities, the weaker jet may not have enough momentum to penetrate the wall jet created by its partner and is deflected before impingement.

A guide to interpreting results obtained by visualizing the flow from below is provided in Fig. 4. The photographs are representative of jet impingement and interaction. Wall jet regions to the far left and right of the impinging jets (1) appear black with bright streaks (striations) indicating that the free surface is predominantly smooth with intermittent irregularities. For the smaller impingement velocity, the wall jets appear *glass-like* to the eye, revealing fewer striations and indicating a smoother air–water interface. In the impingement regions (2) for $\bar{V}_j = 2.1$ m s$^{-1}$, narrow bright lines can be seen to extend across the width of the plate, delineating the curved free surfaces of the jets as they impinge. For $\bar{V}_j = 4.5$ m s$^{-1}$, the lines are broadened to bands in which conditions appear mottled. Part of what is seen in the photograph is the free surface of the jet descending to the plate (3), as visualized from inside the jet. The mottled texture is due to ripples in the jet's free surface, which are typical of higher velocity flows issuing from a planar nozzle [13, 14]. Conversely, for the lower velocity, the falling jet's free surface (3) is smooth (glass-like) and appears black in contrast to the curve free surface at impingement (2). For the higher velocity, a distinction between regions (2) and (3) is not readily made because both regions bend light toward the camera. The darker region (4), seen distinctly for the higher velocity, is a view into the nozzle exit. For the lower velocity, neither region (3) nor (4) reflects light, precluding their delineation. In some of the photographs, bright, clearly defined regions appeared immediately next to the jets (5) and resulted from light transmitted by the jet guards.

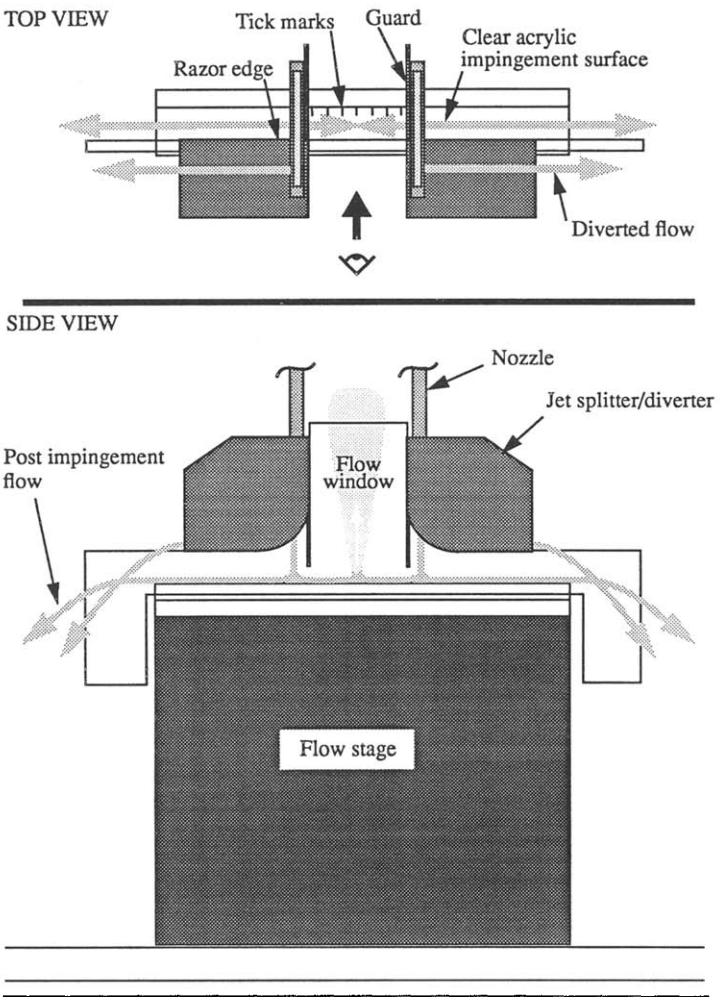


FIG. 3. Flow stage/window assembly used for visualization from the side.

Region (6) appears bright because the interaction fountain reflects a good deal of light through the wall jets. The striations, which represent reflected light toward the camera in region (1), now appear as dark lines against the bright background. Likewise, in region (7), the curved surfaces of the upwelling fountain shade the camera from light which is reflected from above. Region (8) which appears lighter than (7), is a direct view of the maelstrom resulting from the interaction.

## RESULTS AND DISCUSSION

*Single jets*

Figure 5 provides heat transfer coefficient distributions for a single impinging jet. Reported stagnation heat transfer coefficients match a correlation proposed by Wolf *et al.* [14] to within 5%. That correlation is

$$h_0 = 0.116(k/w_j)Re_j^{0.71}Pr^{0.4}. \quad (3)$$

Downstream local coefficients typically agree with the correlations of Wolf *et al.* to within 12%. The correspondence is well within the experimental uncertainty and is to be expected since nearly identical nozzles were used. Due to development of a laminar boundary layer, there is a sharp reduction in the local convection coefficient after impingement. Transition to turbulence subsequently increases the coefficient, providing a local maximum as the turbulent thermal boundary layer thickens. Average heat transfer coefficients were determined over a region which extended 81 mm from the stagnation line and corresponded to the larger pitch used in the dual jet experiments.

*Twin planar jets*

For a guarded system, twin planar jets ($V^* = 1$) generate highly repeatable and nearly symmetric conditions about an interaction zone which is midway between the jets (Fig. 6). The fountain rises approximately 100 mm from the plate for $\bar{V}_j = 2.1$ m s$^{-1}$

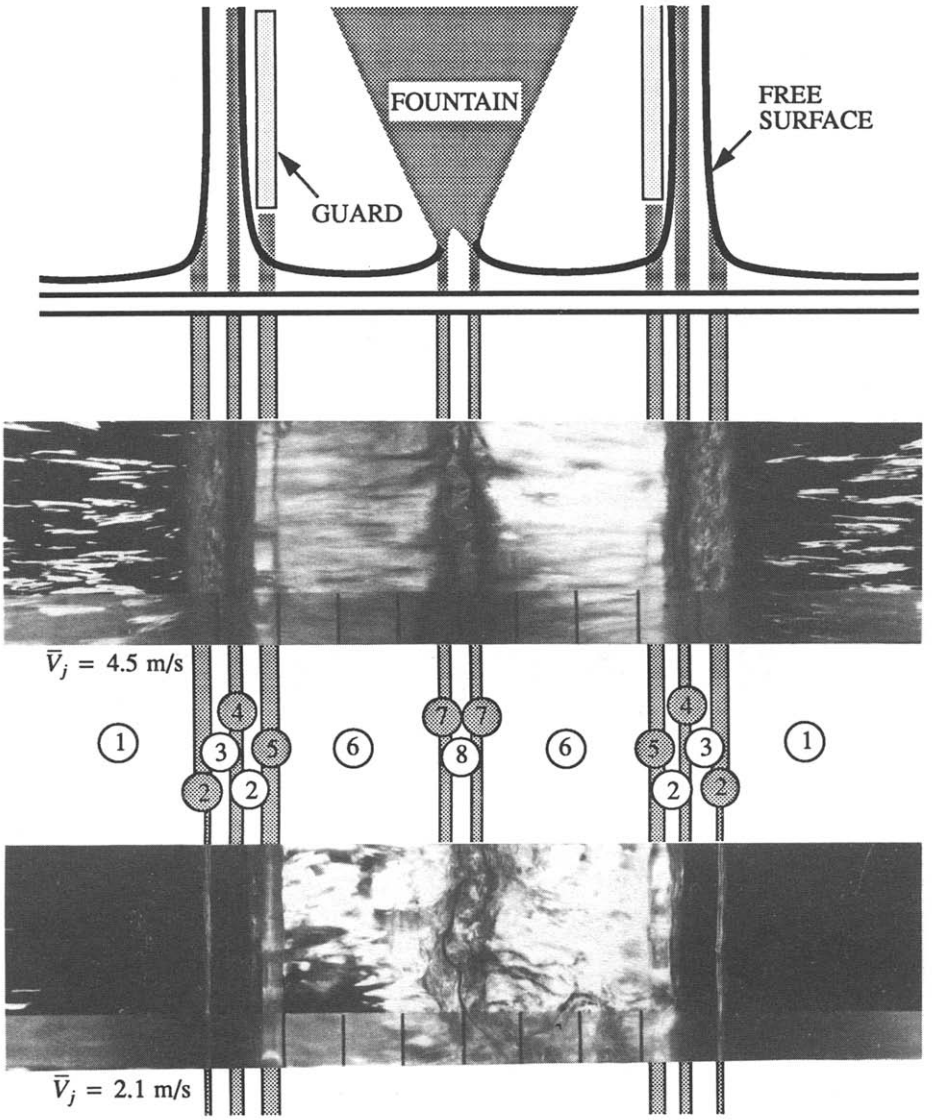


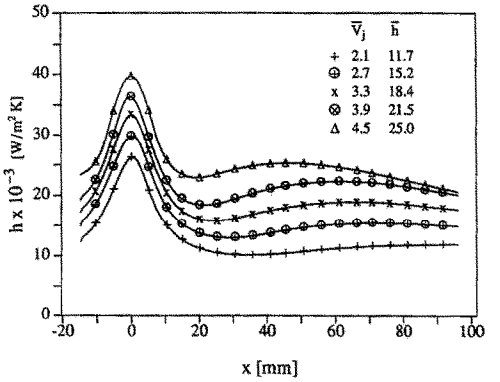


FIG. 5. Local heat transfer coefficient distributions for single planar jet impingement.

(Fig. 7), and nearly 800 mm for $\bar{V}_j = 4.5$ m s$^{-1}$. With increasing fountain height, more of the spent flow falls clear of the plate. For the larger velocity, the interaction zone oscillates by less than 5 mm in either direction, and the amplitude of the oscillation increases with decreasing $\bar{V}_j$ to a maximum of approximately 10 mm at 2.1 m s$^{-1}$. This behavior is attributed to the increasing effect which reimpinging spent flow from the fountain has on the wall jets with decreasing impingement velocity.

For the unguarded systems (Fig. 6), the impingement zones become progressively more obscure with decreasing $\bar{V}_j$ as the interaction fountain careens back and forth, alternately impacting the unprotected jets. Moreover, as manifested by more intense and random

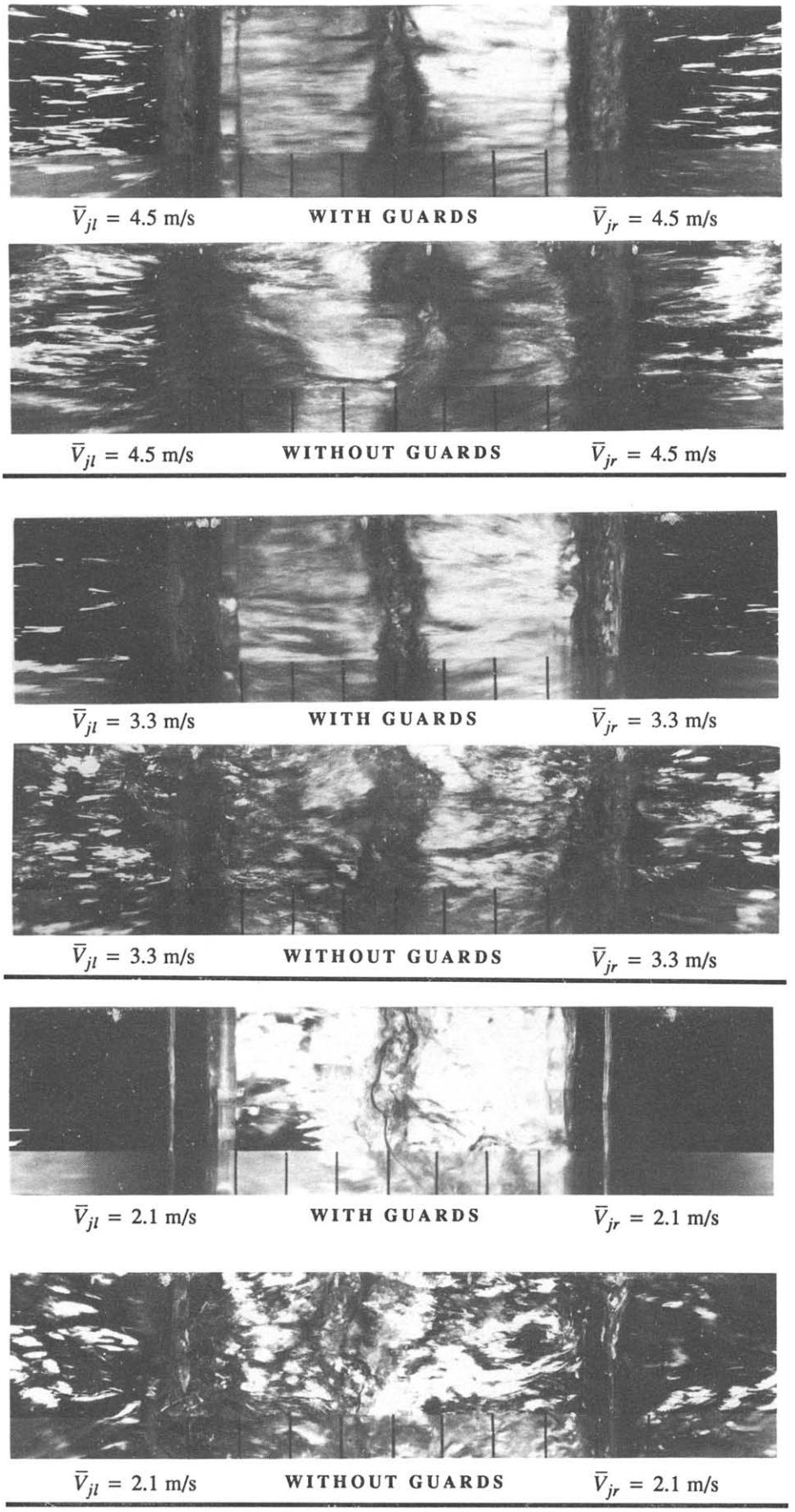


FIG. 6. Twin planar jets viewed from below ($P$ = 81 mm).

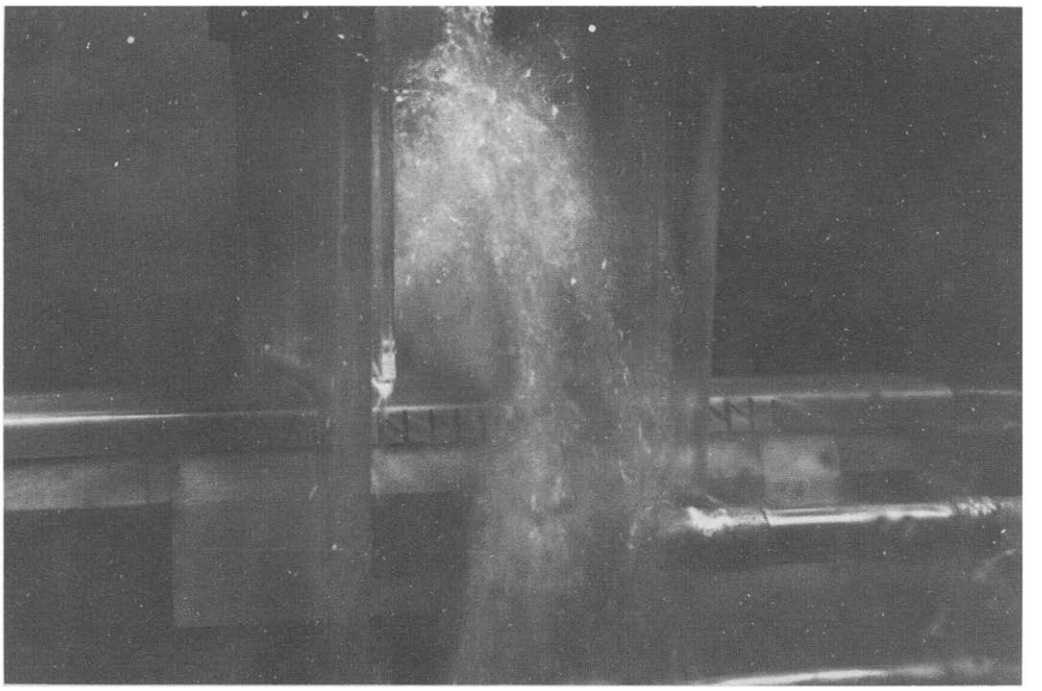

FIG. 7. Photograph of twin planar jets and the interaction fountain for $\bar{V}_{jl} = \bar{V}_{jr} = 2.1$ m s$^{-1}$.

striations in the wall jets on either side of the impingement zones, the free surfaces of the wall jets are affected by droplets which originate from the interaction fountain and strike both the impinging and wall jets.

Local convection heat transfer coefficient distributions beneath the twin planar jets are shown in Fig. 8. The origin is prescribed at the midline of one jet (arbitrarily defined as the *left jet*), placing the midline of the *right jet* at $x = P = 81$ mm. A prominent feature of the guarded data is the existence of a maximum at $x = 40$ mm, which is comparable to values in the stagnation regions. Visualization from below (Fig. 6) identified $x = 40$ mm as the center of the interaction zone, where the wall jets experienced deceleration parallel to and marked separation from the plate.

Removal of the guards has the expected effect of providing a more uniform distribution, even in the impingement regions, where the impingement momentum is reduced as the interaction fountain alternately strikes the jets. The time-averaged impingement heat transfer coefficients are thereby reduced and shifted outward. Due to large oscillations of the interaction zone, heat transfer in the wall jet regions is enhanced, just as heat transfer at $x = 40$ mm is reduced. This time-averaged effect creates a nearly uniform distribution between the impinging jets, with a slight maximum remaining at $x = 40$ mm. The spatially averaged heat transfer coefficient is only slightly influenced by the guards, with the chaos induced by their absence providing weak enhancement. However, differences are within the experimental uncertainty.

Two of the foregoing distributions are compared to results for a single jet in Fig. 9. With the guards, the distributions agree well in the common impingement region ($x = 0$) and in the corresponding wall jet region up to $x = 25$ mm. However, the dual jets provide enhancement in the interaction zone ($30 \leqslant x \leqslant 50$ mm) and in the second (right) wall jet and impingement regions ($70 \leqslant x \leqslant 90$ mm). However, the effect on $\bar{h}$ is not pronounced, particularly for $\bar{V}_j = 4.5$ m s$^{-1}$. Although the relative amount of spent flow from

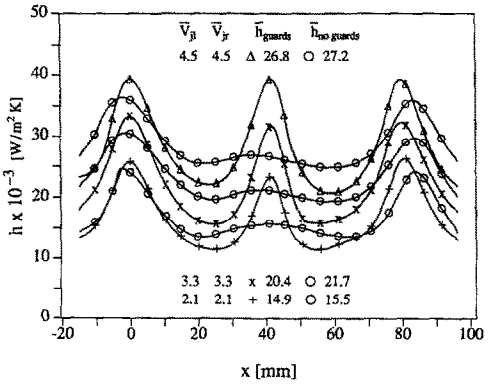


FIG. 8. Local heat transfer coefficient distributions for twin planar jets ($P = 81$ mm).

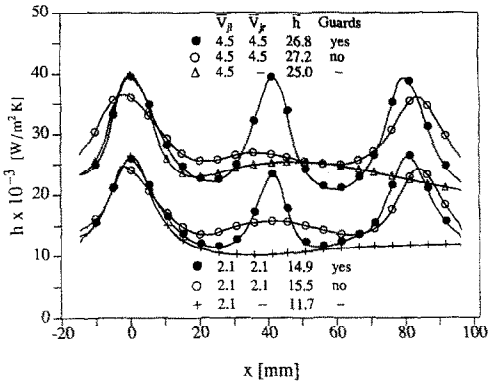


FIG. 9. Comparison of local heat transfer coefficient distributions for twin planar jets and a single planar jet ($P = 81$ mm).

the fountain which impacts the wall jets increases with decreasing impingement velocity, this *reimpingement* does not enhance heat transfer in much of the wall jet region. Droplets associated with the spent flow apparently lack the momentum to fully penetrate the wall jets, or otherwise significantly affect heat transfer.

With a reduction in the nozzle pitch from 81 to 51 mm, flow observations made from below did not differ significantly from those depicted in Fig. 6, except that the equilibrium position of the wall jet interaction zone was located at $x_c \approx 25$ mm, instead of at 40 mm. However, as shown in Fig. 10, a reduction in length of the wall jet region increases the average heat transfer coefficient. Because the size of the impingement region is unaffected by pitch, the impingement zone now occupies what were wall jet transitional regions for the larger pitch. For $P = 81$ mm, wall jet interactions do not begin to enhance heat transfer until $x \approx 25$ mm; for $P = 51$ mm this distance is reduced to $x \approx 15$ mm, thus circumventing boundary layer growth.

There are two other noteworthy features of twin planar jets, both of which pertain to unguarded conditions. The first is that heat transfer enhancement

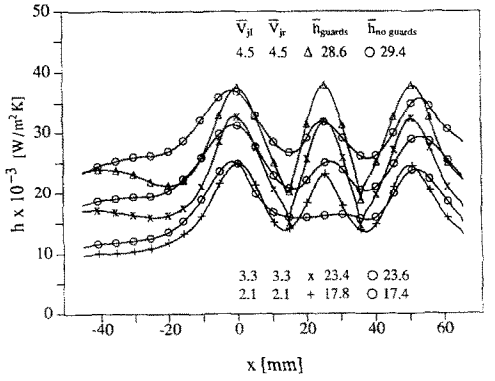


FIG. 10. Local heat transfer coefficient distributions for twin planar jets ($P = 51$ mm).

exists outside of the unguarded jets ($x < 0$ and $x > P$). Although this condition exists for both values of $P$, it is most evident in Fig. 10, simply because more data are available for $x < 0$. Enhancement is due to impingement of the unprotected free-surface jets by the interaction fountain. While convection coefficients are slightly reduced by the disturbance in the impingement zone, the ensuing laminar boundary layer is turbulated and heat transfer is enhanced. Enhancement is limited to the wall jet laminar/transition region associated with use of the guards and disappears with development of a turbulent boundary layer. Note, however, that such conditions would be altered if there were more than two nozzles in the array, with placement at $x = -P$ and $x = 2P$. The other feature pertains to local convection coefficients in the interaction zone. Although such coefficients are unaffected by pitch when the jets are guarded, it is evident from Figs. 8 and 10 that more pronounced interaction peaks exist at the higher velocities for $P = 51$ mm, implying the existence of a more stable interaction zone. Based on flow visualization from the side, this increased stability is attributed to the height of the fountain. When the nozzles were close, droplets descending from the fountain, which would have otherwise impacted the unprotected free-surface jets, instead struck the nozzles, reducing their disruptive influence and permitting the establishment of a more stable interaction zone. For $\bar{V}_j = 2.1$ m s$^{-1}$, the interaction zone is not stabilized in this manner because the apex of the fountain only extends approximately 10 mm above the nozzle discharge. Hence, the nozzles do not shield the free surface jets and, in fact, the smaller pitch destabilizes the flow by bringing the free-surface jets closer to droplets ejected from the weaker fountain. The heat transfer coefficient distribution in the region between the jets is accordingly flattened.

*Unequal planar jets*

As the jet impingement velocity ratio was decreased from unity, guarded jet impingement systems retained well behaved, clearly defined flow fields (Fig. 11). Although the interaction zone shifted towards the weaker jet with decreasing $V^*$, stable oscillatory conditions were maintained about a new equilibrium position. Flow fields were therefore similar to those for the twin systems, so long as the interaction zone remained sufficiently far from the weaker jet. However, when the velocity ratio was reduced to $V^* = 0.67$ ($\bar{V}_{jr} = 3.0$ m s$^{-1}$), this was no longer the case. The interaction zone moved so close to the right jet that its oscillations placed it within the impingement zone. At this point the jet guard could not prevent the weaker jet from being overwhelmed, and it served only to intrude upwelling of fluid at the inner face of the weaker jet. Because the interaction zone could no longer be stabilized by guarding the free-surface jets, the guarded jet condition was not studied for $V^* < 0.67$ and $P = 81$ mm.

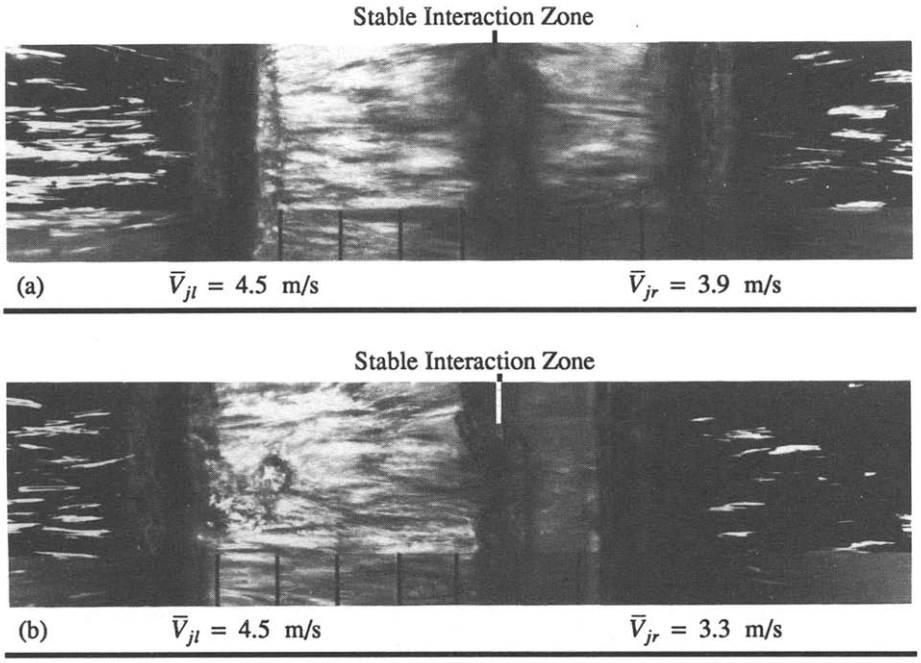


FIG. 11. Unequal planar jets with guards viewed from below ($P$ = 81 mm): (a) $V^*$ = 0.87, (b) $V^*$ = 0.73.

When jet guards were not used, flow conditions were characterized by a unique oscillation. When the interaction zone attempted to assume an equilibrium position, the fountain preferentially disrupted the weaker jet due to its close proximity, momentarily overwhelming the jet and subsequently receding from the jet. The process repeated itself, and instead of careening back and forth between well defined free-surface jets, as in a twin jet system, the interaction zone repeatedly struck the weaker jet. The effect of removing the guard may be seen by contrasting Figs. 11(a) and 12(a). Although an interaction zone existed for $V^* = 0.73$, its location was not fixed. The dynamic behavior of the interaction zone is shown in the sequential photographs of Fig. 12(b). With decreasing velocity ratio, the weaker jet was able to impinge from time to time, forming a partial interaction zone, but was typically overcome by the stronger jet (Fig. 12(c)). For $V^* = 0.47$, an interaction zone was never observed.

Heat transfer coefficient distributions associated with unequal jets are shown in Fig. 13. When guards are used, there is significant enhancement within the interaction zone, which shifts progressively further to the right with decreasing $V^*$ (Figs. 13(a), (b)). Conditions to the left of this zone are uninfluenced by the weaker jet, while coefficients in the impingement region of the weaker jet are reduced slightly, as the interaction zone draws closer. This reduction is attributed to crossflow effects generated as the oscillating interaction zone interrupts impingement more frequently.

Convection coefficient distributions for the unguarded condition reveal the effect of interactions between the weaker jet and the fountain. For $V^* = 0.87$ (Fig. 13(a)), the weaker jet is able to sustain an impingement zone and a distinct wall jet interaction region. The result is a weak maximum at $x \approx 65$ mm, which is a quasi-equilibrium position about which the interaction zone oscillates. The effects of the oscillation are also seen in the impingement zone, where coefficients are reduced by the crossflow. However, beyond the weaker jet ($x \gtrsim 85$ mm), crossflow acts to enhance heat transfer. For $V^* = 0.74$ (Fig. 13(b)), there is no longer a local maximum associated with the interaction zone and its oscillation acts to degrade heat transfer in the impingement zone, while enhancing heat transfer beyond this zone. For $V^* \lesssim 0.60$, the weaker jet is overwhelmed by the crossflow imposed by the stronger jet, and heat transfer is only marginally enhanced in proximity to the weaker jet (Fig. 13(c)).

Once again, average heat transfer coefficients are relatively unaffected by the presence or absence of guards. Although the time-averaging effect of a less stable interaction zone produces a more uniform distribution of local coefficients, the total heat transfer remains approximately the same. Moreover, the weaker jet has a negligible effect on the average coefficient for $V^* \lesssim 0.87$, irrespective of whether guards are deployed.

Convection coefficient distributions for a nozzle spacing of 51 mm are shown in Fig. 14. For $V^* = 0.87$ (Fig. 14(a)), the interaction zone is centered about $x_e \approx 33$ mm and is characterized by a prominent maximum for both the guarded and unguarded con-

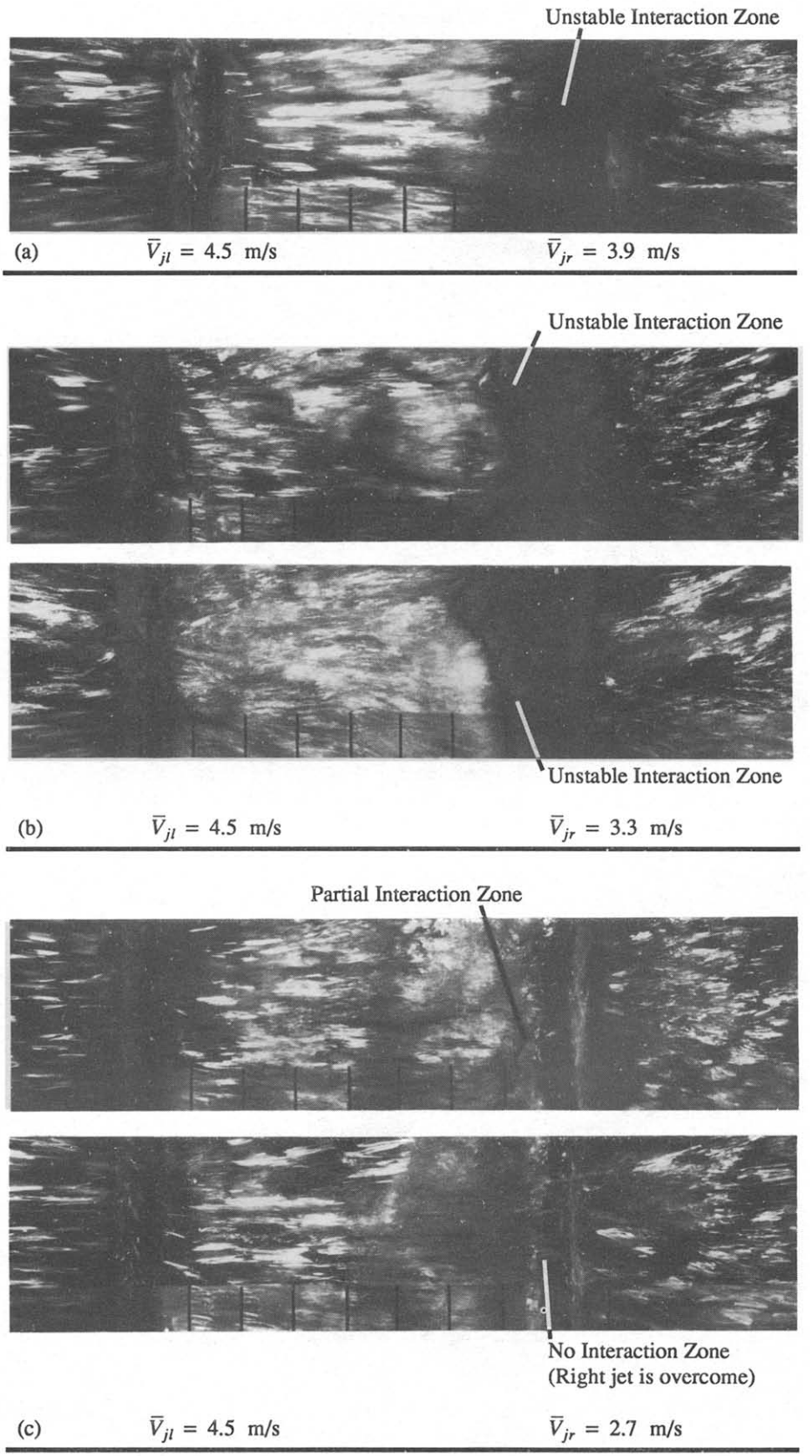


FIG. 12. Unequal planar jets without guards viewed from below ($P$ = 81 mm): (a) $V^*$ = 0.87, (b) $V^*$ = 0.73, (c) $V^*$ = 0.60.

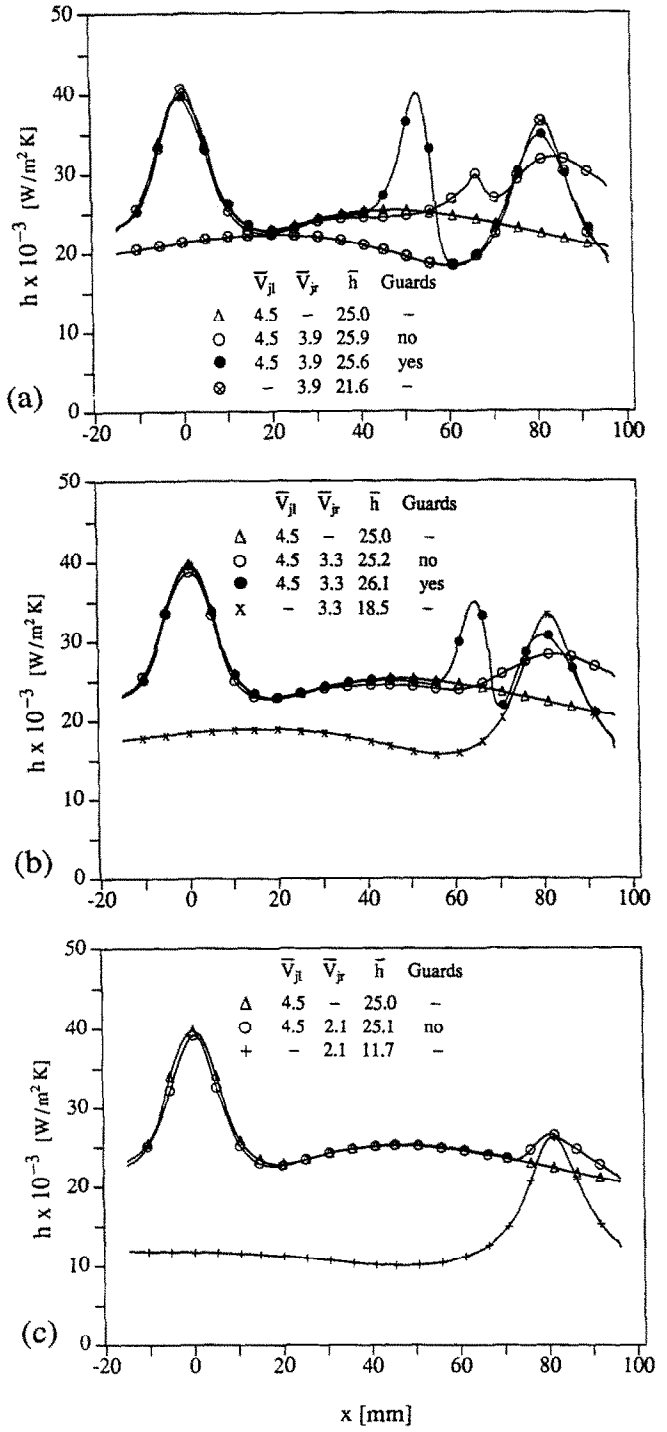


FIG. 13. Local heat transfer coefficient distributions for unequal planar jets ($P = 81$ mm): (a) $V^* = 0.87$, (b) $V^* = 0.73$, (c) $V^* = 0.47$.

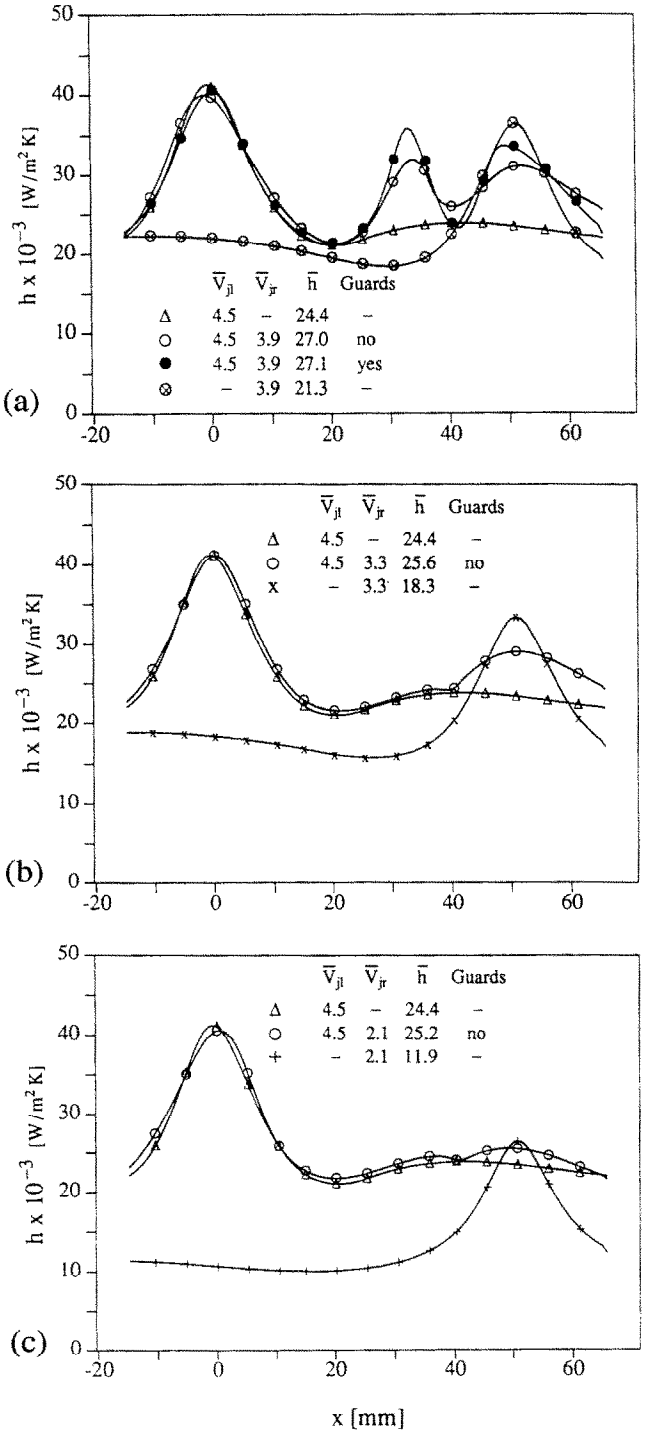


FIG. 14. Local heat transfer coefficient distributions for unequal planar jets ($P = 51$ mm): (a) $V^* = 0.87$, (b) $V^* = 0.73$, (c) $V^* = 0.47$.

ditions. Relative to values for a single jet, convection coefficients in the impingement region of the weaker jet are reduced, particularly for the unguarded condition. Beyond this region ($x \gtrsim 55$ mm), there is some enhancement relative to heat transfer for a single jet, even with the guard. This behavior reflects the increasing influence of the interaction fountain on the weaker jet with decreasing $P$. For $x \lesssim 20$ mm, heat transfer coefficients match those of the single (stronger) jet. The usefulness of the jet guards again diminished with decreasing $V^*$, and for $P = 51$ mm became nonexistent at $V^* \approx 0.83$ (in contrast to $V^* \approx 0.67$ for $P = 81$ mm). For $V^* = 0.74$ (Fig. 14(b)), the oscillating interaction zone encroached on the impingement zone of the weaker jet, providing some enhancement relative to a single (stronger) jet, but yielding coefficients which are lower than those associated with an independent weaker jet. For $V^* = 0.47$ (Fig. 14(c)), the weaker jet had a negligible effect on the distribution associated with the stronger jet. In this case the crossflow imposed by the stronger jet was sufficient to deflect the weaker jet and to nearly eliminate the effects of impingement on surface conditions.

For $V^* = 0.87$ (Fig. 14(a)), the average coefficient is enhanced by the weaker jet, and because the impingement and interaction zones occupy a larger fraction of the surface area between the jets, average coefficients exceed those for $P = 81$ mm (Fig. 13(a)). At lower velocity ratios, however, average coefficients are determined principally by the strong jet and the effect of the pitch becomes negligible.

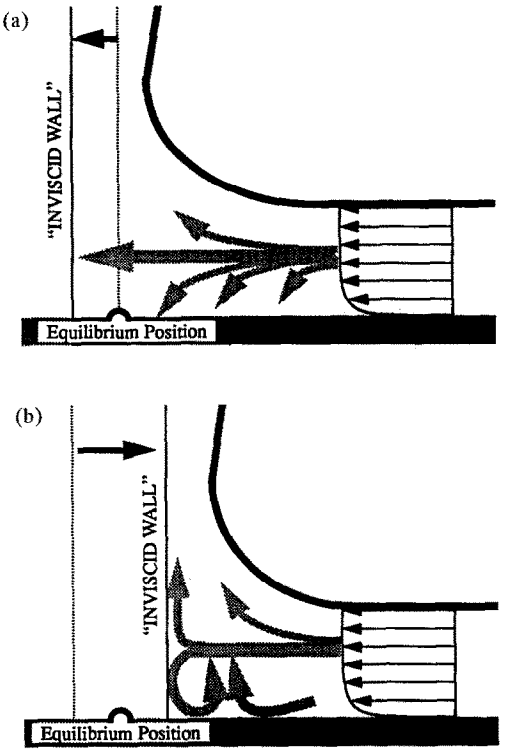


FIG. 15. Possible contribution of oscillation about an equilibrium position to thermal boundary layer thinning and enhanced mixing within a wall jet interaction zone: (a) line of collision shifts to the left at the free-stream velocity and cooler free-stream fluid tumbles to the plate in place of slower boundary layer flow; (b) line of collision shifts to the right and flow reversal routes high-momentum, free-stream fluid to the plate.

*Enhanced heat transfer in the interaction zone*

Heat transfer enhancement observed in the interaction zone of colliding wall jets is an important result of this study and merits further discussion. In particular, enhancement is believed to be strongly influenced by the oscillatory nature of the interaction zone.

Consider one of the interacting wall jets to be separated from the opposing jet by a hypothetical moving vertical plane which is assumed to be impenetrable but along which a zero-shear flow may occur (Fig. 15). Oscillation of such an *inviscid wall* suggests a mechanism by which cool free-stream fluid could be routed from the wall jet to the heated surface. If the barrier moves to the left at the free-stream velocity, the slower boundary layer flow will not keep pace; and the faster free-stream fluid will descend to the surface in its place (Fig. 15(a)). As the inviscid wall moves back to the right (Fig. 15(b)), high-momentum, free-stream fluid may experience flow reversal, briefly driving a small recirculation cell at approximately the free-stream velocity. Repetition of the foregoing events would create conditions for which there is strong mixing and intermittent disruption of the thermal boundary layers in the interaction zone between opposing wall jets.

Intermittency in impinging liquid jets has recently been considered by Zumbrunnen and Aziz [15] and has been shown to provide heat transfer enhancement in the impingement and wall jet regions due to a boundary layer renewal process. The method involves a high frequency interruption of the flow, which repeatedly initiates transient heat transfer to a newly developing boundary layer. Relative to steady state conditions, heat transfer rates are enhanced during this transient, but are reduced in the brief period of time when the flow is stopped. When the frequency is sufficiently high ($\sim 100$ Hz), benefits outweigh the penalties of a disrupted flow and there is a net increase in heat relative to steady impingement. Although the interaction zones of this study oscillate at a much lower frequency ($\sim 1$ Hz), boundary layer renewal and intermittent exposure to cooler, free-stream fluid may still make an important contribution to heat transfer enhancement.

## CONCLUSIONS

Experiments have been performed to determine flow conditions and convection heat transfer distributions associated with two planar, free-surface jets. Although the jet width and nozzle-to-plate distance were fixed, impingement velocities and the nozzle pitch were varied. For twin planar jets (equivalent

impingement velocities) with guards, the quasi-equilibrium position of a well-defined, oscillating interaction zone is midway between the impingement points. The zone is characterized by a *fountain* which results from the interacting wall jets. Outside the interaction zone, local heat transfer coefficients associated with one jet are largely unaffected by the other jet. Within the stable interaction zone, there is a local maximum in the heat transfer coefficient which is comparable to values associated with impingement. Removal of the guards produces a more unstable flow field which extends the influence of the interaction zone to all locations between the jets. The local maximum in the convection coefficient is reduced, while coefficients for adjoining regions are enhanced.

Hydrodynamically, reduction of the ratio of impinging jet velocities from unity shifts the quasi-equilibrium position of the interaction zone toward the weaker jet. In terms of heat transfer, stable fountains resulting from guarded, unequal jets still produce their characteristically high peaks. However, as the interaction zone approaches the weaker jet, the jet guard loses its efficacy and a stable fountain is not possible. The peak coefficient in the interaction zone is reduced, and eventually eliminated, while convection coefficients in adjoining regions are enhanced.

The ability of stable interaction zones to support levels of heat transfer comparable to those for jet impingement was demonstrated for both of the nozzle pitches studied. When guards are not used and the velocities are such as to produce an interaction fountain rising higher than the nozzle exits, decreased nozzle pitch is observed to have a stabilizing influence on the flow fields of unguarded planar jets. The nozzles act to guard the free jets from droplets falling from the fountain, the larger peaks are consequently achieved at the equilibrium position.

*Acknowledgements*—Funding for this research was provided by the National Science Foundation under Grant CTS-8912831.

## REFERENCES

1. H. Martin, Heat and mass transfer between impinging gas jets and solid surfaces. In *Advances in Heat Transfer* (Edited by J. P. Hartnett and T. F. Irvine), Vol. 13, pp. 1–60. Academic Press, New York (1977).
2. R. Gardon and J. Cobonpue, Heat transfer between a flat plate and jets of air impinging on it. In *Proceedings of the 2nd International Heat Transfer Conference*, pp. 454–460. ASME, New York (1962).
3. M. Korger and F. Křížek, Mass-transfer coefficient in impingement flow from slotted nozzles. *Int. J. Heat Mass Transfer* **9**, 337–344 (1966).
4. R. Gardon and J. C. Akfirat, Heat transfer characteristics of impinging two-dimensional air jets. *J. Heat Transfer* **88**, 101–108 (1966).
5. R. N. Koopman and E. M. Sparrow, Local and average transfer coefficients due to an impinging row of jets. *Int. J. Heat Mass Transfer* **19**, 673–683 (1976).
6. N. R. Saad, A. S. Mujumdar and W. J. M. Douglas, Heat transfer under multiple turbulent slot jets impinging on a flat plate. In *Drying '80* (Edited by A. S. Mujumdar), Vol. 1, pp. 422–430. Hemisphere, New York (1980).
7. S. Mikhail, S. M. Morcos, M. M. M. Abou-Ellail and W. S. Ghaly, Numerical prediction of flow field and heat transfer from a row of laminar slot jets impinging on a plate. In *Proceedings of the 7th International Heat Transfer Conference* (Edited by U. Grigull, E. Hahne, K. Stephan and J. Straub), Vol. 3, pp. 337–382. Hemisphere, New York (1982).
8. A. I. Behbahani and R. J. Goldstein, Local heat transfer to staggered arrays of impinging circular air jets. *J. Power* **105**, 354–360 (1983).
9. S. Ishigai, S. Nakanishi, M. Mizuno and T. Imamura, Heat transfer of the impinging round water jet in the interference zone of the film flow along the wall. *Bulletin JSME* **20**, 85–92 (1977).
10. D. T. Vader, F. P. Incropera and R. Viskanta, A method for measuring steady, local heat transfer to an impinging liquid jet. *Exp. Thermal Fluid Sci.* **4**, 1–11 (1991).
11. R. J. Moffat, Describing the uncertainties in experimental results. *Exp. Thermal Fluid Sci.* **1**, 3–17 (1988).
12. D. A. Zumbrunnen, F. P. Incropera and R. Viskanta, A method and apparatus for measuring heat transfer distributions on moving and stationary plates cooled by a planar liquid jet. *Exp. Thermal Fluid Sci.* **3**, 202–213 (1990).
13. D. T. Vader, F. P. Incropera and R. Viskanta, Convection nucleate boiling on a heated surface cooled by an impinging, planar jet of water. *J. Heat Transfer* **114**, 153–160 (1992).
14. D. H. Wolf, R. Viskanta and F. P. Incropera, Local convective heat transfer from a planar jet of water with a non-uniform velocity profile. *J. Heat Transfer* **112**, 899–905 (1990).
15. D. A. Zumbrunnen and M. Aziz, Convective heat transfer enhancement due to intermittency in an impinging jet. *J. Heat Transfer* **115**, 91–98 (1993).